A theory of mode of action of azolylalkylquinolines as DNA binding agents using automated flexible ligand docking

Armin Madadkar Sobhani [a],*, Sara Rasoul Amini [b], Joel D.A. Tyndall [c],
Ebrahim Azizi [d], Mohsen Daneshtalab [e], Ali Khalaj [b]

[a] Computational Chemistry Lab., Razi Institute for Drug Research, Iran University of Medical Sciences, Iran
[b] Department of Medicinal Chemistry, School of Pharmacy, Tehran University of Medical Sciences, Tehran, Iran
[c] National School of Pharmacy, University of Otago, New Zealand
[d] Molecular Research Lab., Department of Pharmacology and Toxicology, School of Pharmacy,
Tehran University of Medical Sciences, Tehran, Iran
[e] School of Pharmacy, Memorial University of Newfoundland, St. John's, Canada

Abstract

Azolylalkylquinolines (AAQs) are a family of quinolines with varying degrees of cytotoxic activity (comparable or moderately superior to adriamycin in some cases) developed in the past decade in our group where their exact mode of action is still unclear. In this study the most probable DNA binding mode of AAQs was investigated employing a novel flexible ligand docking approach by using AutoDock 3.0. Forty-nine AAQs with known experimental inhibitory activity were docked onto d(CGCAAATTTGCG)$_2$, d(CGATCG)$_2$ and d(CGCG)$_2$ oligonucleotides retrieved from the Protein Data Bank (PDB IDs: 102D, 1D12 and 1D32, respectively) as the representatives of the three plausible models of interactions between chemotherapeutic agents and DNA (groove binding, groove binding plus intercalation and bisintercalation, respectively). Good correlation ($r^2 = 0.64$) between calculated binding energies and experimental inhibitory activities was obtained using groove binding plus intercalation model for phenyl-azolylalkylquinoline (PAAQ) series. Our findings show that the most probable mode of action of PAAQs as DNA binding agents is via intercalation of quinolinic moiety between CG base pairs with linker chain and azole moiety binding to the minor groove.
© 2006 Elsevier Inc. All rights reserved.

Keywords: Molecular docking; DNA binding; Cytotoxic quinolines; AutoDock; HIN2PDBQS

1. Introduction

A series of azolylalkylquinolines (AAQs) have been previously developed in our group as potent and selective cytotoxic agents in vitro [1–5], of which some compounds (e.g. N-[4-quinolyl]-azolylalkyl-amines) have exhibited activity comparable or moderately superior to adriamycin (doxorubicin). Because our group is also interested in structure-based rational design of the above-mentioned AAQs, elucidating a mechanism for their action is crucial for further improvements of their structure. Preliminary mechanistic studies revealed that these compounds act in a concentration-dependent manner and some of them were active against topoisomerases type I and type II [3].

Based on the previous report that suggests the alkyl-linked 4-aminodiquinolines act as monofunctional intercalators [6], in this study we placed the DNA binding capabilities of these compounds under scrutiny using a novel in silico approach.

DNA represents one of the most important molecular–cellular targets of several chemotherapeutic drugs. Chemotherapeutic agents targeting DNA can be conveniently categorized, depending on their mode of interaction, into two major classes [7]: (i) covalent binding, and (ii) noncovalent binding, including intercalative binding and DNA major- and minor-groove-binding. Polycyclic heterocycles having a planar structure can be effective pharmacophore moieties of DNA-intercalative agents because they can insert between the stacked base pairs of oligonucleotides. Moreover if they bear suitable side chains, further interactions of these ligands with the other important architectural features of DNA, e.g. minor groove, can be envisaged.

---

* Corresponding author. Tel.: +98 21 8805 2265; fax: +98 21 8805 2264.
E-mail address: armin@iums.ac.ir (A.M. Sobhani).

Table 1
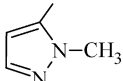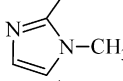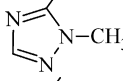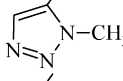Chemical structure of the 49 azolylalkylquinolines studied
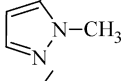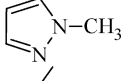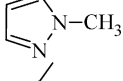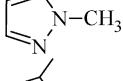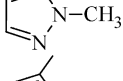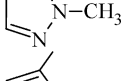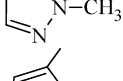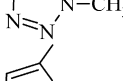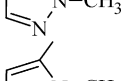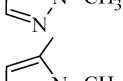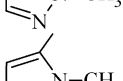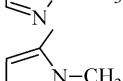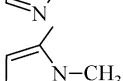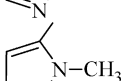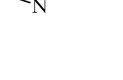
Compound	Group	X	n	Azole	Pos[a]	R
M1	MAAQ	S	6		4	2-H
M2	MAAQ	O	6		4	2-H
M3	MAAQ	O	6		4	2-H
M4	MAAQ	O	6		4	2-H
M5	MAAQ	O	6		4	2-H
M6	MAAQ	O	7		4	2-H
M7	MAAQ	O	8		4	2-H
M8	MAAQ	O	10		4	2-H
M9	MAAQ	O	11		4	2-H
M10	MAAQ	NHCO	10		4	2-H
M11	MAAQ	N	5		4	2-H
M12	MAAQ	N	6		4	2-H
M13	MAAQ	N	6		4	2-H
M14	MAAQ	N	6		5	2-H
M15	MAAQ	N	6		8	2-H
M16	MAAQ	N	7		4	2-H
M17	MAAQ	N	7		4	7-CF$_3$
M18	MAAQ	N	8		4	2-H
M19	MAAQ	N	10		4	2-H

Table 1 (*Continued*)
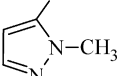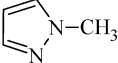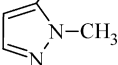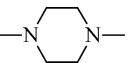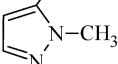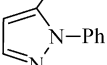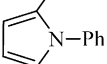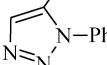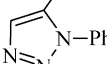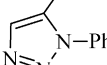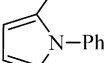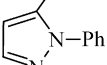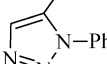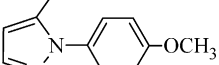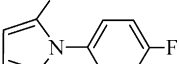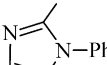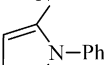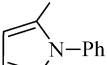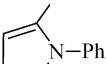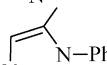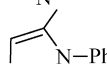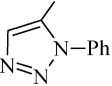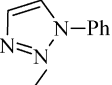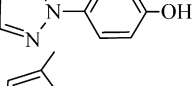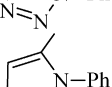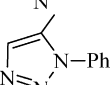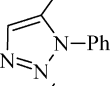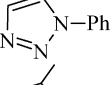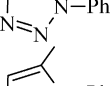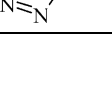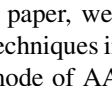
Compound	Group	X	n	Azole	Pos[a]	R
M20	MAAQ	CONH	7		4	2-H
M21	MAAQ	CONH	10		4	2-H
M22	MAAQ	CH(CH₂)O	10		4	2-H
M23	MAAQ	—N(piperazine)N—	6		4	2-H
P1	PAAQ	S	6		4	2-H
P2	PAAQ	S	6		4	2-H
P3	PAAQ	S	8		4	2-H
P4	PAAQ	S	9		4	2-H
P5	PAAQ	O	5		4	2-H
P6	PAAQ	O	6		4	2-H
P7	PAAQ	O	6		4	2-H
P8	PAAQ	O	6		4	2-H
P9	PAAQ	O	6		4	2-CH₃
P10	PAAQ	O	6		4	2-CH₃
P11	PAAQ	O	6		4	2-CH₃
P12	PAAQ	O	6		4	2-CH₃
P13	PAAQ	O	6		4	2-CH₃
P14	PAAQ	O	6		8	2-H
P15	PAAQ	O	7		4	2-H
P16	PAAQ	O	8		4	2-H

Table 1 (*Continued*)

Compound	Group	X	n	Azole	Pos[a]	R
P17	PAAQ	O	9		4	2-H
P18	PAAQ	O	10		4	2-H
P19	PAAQ	O	10		4	2-H
P20	PAAQ	O	11		4	2-H
P21	PAAQ	O	12		4	2-H
P22	PAAQ	NHCO	6		4	2-H
P23	PAAQ	N	7		4	2-H
P24	PAAQ	N	9		4	2-H
P25	PAAQ	CONH	9		4	2-H
P26	PAAQ	CH(CH$_2$)O	7		4	2-H

[a] Attachment position of the linker chain to the quinoline ring.

Considering the general structure of AAQs (Fig. 1), three structural moieties can be easily recognized: two nitrogen-bearing planar aromatic ring systems (azole and quinoline) separated by an alkyl linker chain. Having these structural groups, there are three plausible modes of interaction with DNA: groove binding, groove binding plus intercalation and bisintercalation.
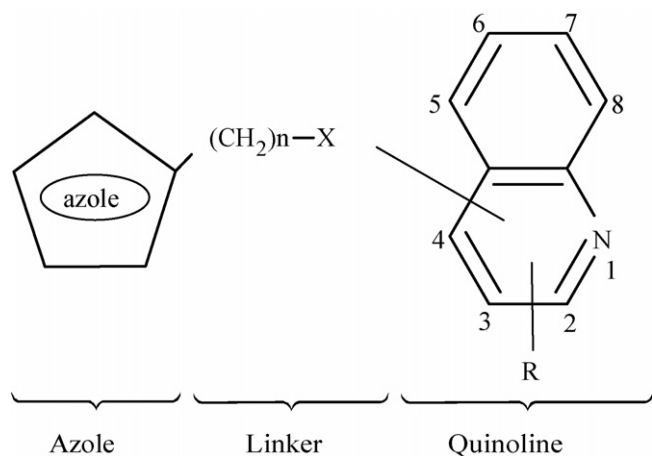
Fig. 1. General structure and numbering used for the 49 azolylalkylquinolines studied.

In this paper, we present application of the flexible ligand docking techniques in order to elucidate the most probable DNA binding mode of AAQs. The crystal structures of three DNA–ligand complexes from the Protein Data Bank (PDB IDs: 102D, 1D12 and 1D32) were selected as the templates for three different types of possible interactions between chemotherapeutic agents and DNA: groove binding, groove binding plus intercalation and bisintercalation, respectively. Forty-nine AAQs categorized into two groups (23 methyl-azolylalkylquinolines or MAAQs; 26 phenyl-azolylalkylquinolines or PAAQs) were docked onto the oligonucleotides extracted from the crystal structures and correlation between calculated binding affinities for each model and experimental values were analyzed to find most satisfying model. A utility program that was used to facilitate some procedures of this work is also reported.

2. Methods

2.1. Preparation of oligonucleotide and ligand molecules

In the simulations we used the crystal structures of three different oligonucleotide–ligand complexes: DNA–propamidine (PDB ID: 102D) [8], DNA–adriamycin (PDB ID: 1D12) [9] and DNA–ditercalinium (PDB ID: 1D32) [10]. The spatial coordinates were retrieved from The Protein Data Bank [11]. For each

PDB file, the ligand and all the water molecules were removed. Missing hydrogens and AMBER95 partial atomic charges were added using HyperChem (HyperCube Inc., Gainesville, FL). By the use of a Win32 based utility named HIN2PDBQS developed in our group, non-polar hydrogens were merged to their corresponding carbons, AMBER95 assigned partial atomic charges were converted to AMBER86 charges and finally desolvation parameters were assigned to each oligonucleotide atom.

For the internal validation phase (see Section 3.3), ligand structures (corresponding HETATM and CONECT records) were extracted from the Protein Databank (pdb) file using a plain text editor. After assigning bond orders, missing hydrogen atoms were added and a short minimization (100 steepest descent steps using MM+ force field with a gradient convergence value of 0.05 kcal/mol Å) was performed using HyperChem in order to release any internal strain. Then in the AutoDockTools package, the partial atomic charges were calculated using Gasteiger–Marsili method [12] and after merging non-polar hydrogens, rotatable bonds were assigned.

For each 49 AAQs listed in Table 1 the same procedure was used as described for internal validation above, except that the
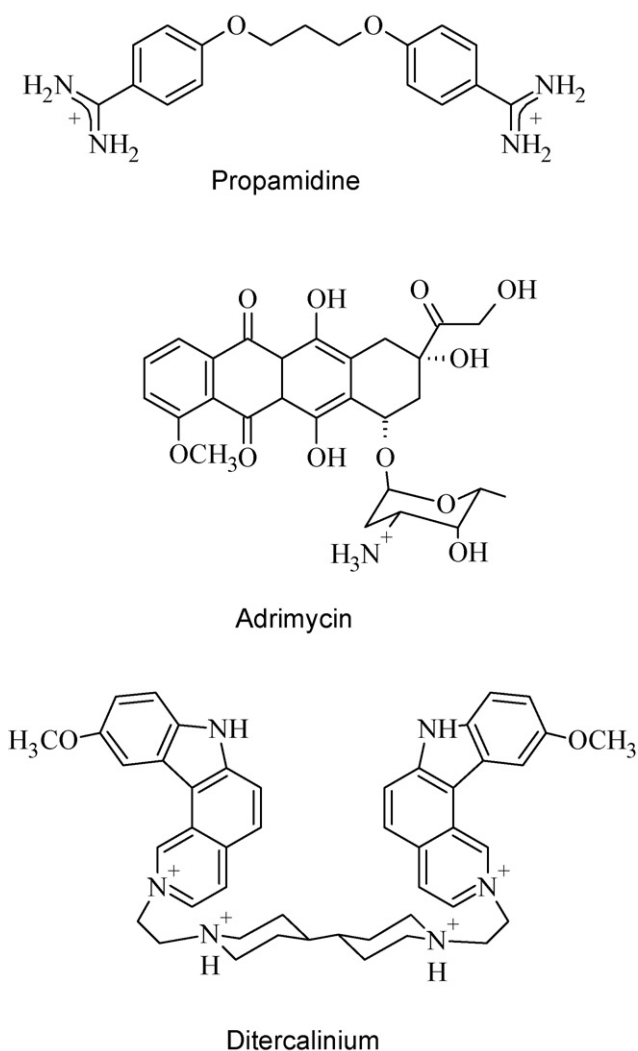
Fig. 2. Chemical strurcutre of the three ligands used in the internal validation phase.
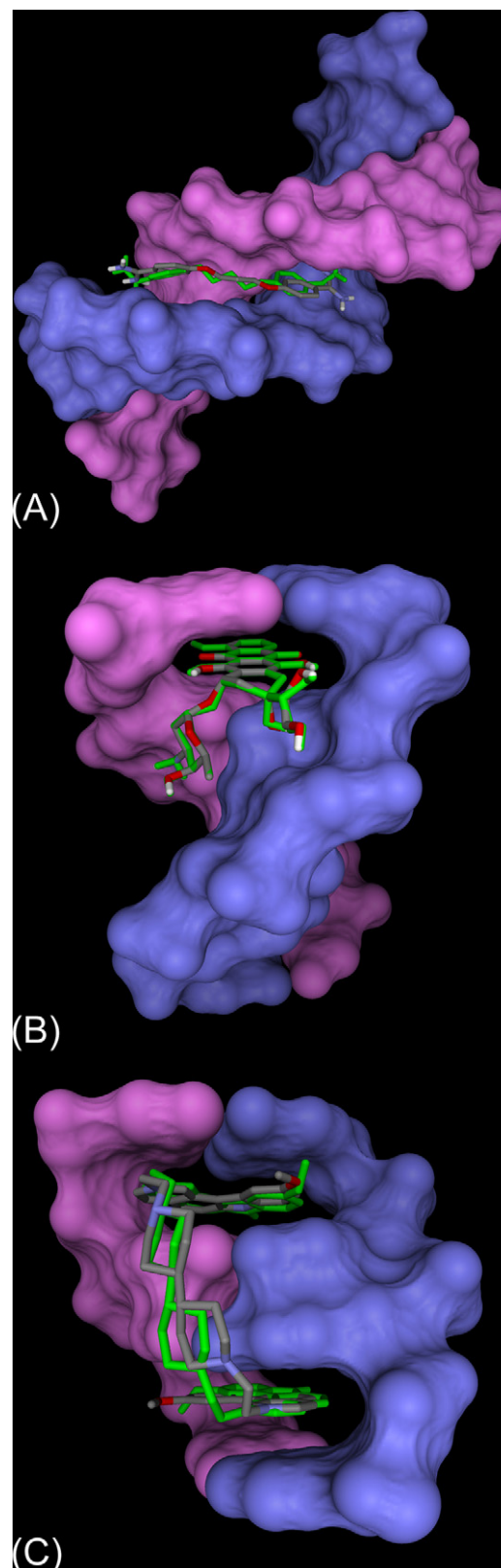
Fig. 3. Internal validation phase results. DNA structure rendered in blue and magenta as solvent-excluded surface (SES). (A) Docking of propamidine (TNT) and conformational comparsion of TNT from crystal structure (colored stick structure) with that from AutoDock model (green). (B) The same for adriamycin (DM1) and (C) ditercalinium (DIT).

3D structures were constructed and optimized using Polak–Ribiere conjugate gradient algorithm and AMBER95 force field implemented in HyperChem.

2.2. Docking protocol

The grid maps representing the DNA in the actual docking process were calculated with AutoGrid (part of the AutoDock package). The grids (one for each atom type in the ligand, plus one for electrostatic interactions) were chosen to be sufficiently large to include not only the active site but also significant portions of the surrounding surface. The points of the grids were thus $60 \times 60 \times 60$ for 102D, and $70 \times 70 \times 70$ for 1D12 and 1D32 with a grid spacing of 0.375 Å (roughly a quarter of the length of a carbon–carbon single bond) and because the location of the original ligand in the complex was known, the cubic grids were centered on the ligand's binding site.

Automated docking studies were carried out using Auto-Dock version 3.0.5 [13]. Of the three different search algorithms offered by AutoDock 3.0, the Lamarckian genetic algorithm (LGA) was applied to model the interaction/binding between DNA and AAQs. For the local search, the so-called pseudo-Solis and Wets algorithm [14] was used. For all docking parameters, standard values were used as described before [13], except the amount of independent docking runs performed for each docking simulation. Multiple docking runs can increase the performance of docking programs [15], as was shown specifically in the case of AutoDock [16]. To meet aspects of calculation time and data size on one hand, and convergence criteria and statistical relevance on the other hand, 50 independent docking runs were performed for each docking case. Cluster analysis was performed on the docked results using a root mean square (RMS) tolerance of 0.5 Å. After ascertaining the robustness of our computational modeling approach in which X-ray structures served as reference structures for the calculation of the root mean square deviation (RMSD), the same modeling computational protocols were applied to AAQs. All calculations were carried out on an Intel Pentium4 2.4 GHz based machine running MS Windows XP SP2 as operating system and a modified version of AutoDock/AutoGrid that can be natively compiled in Win32 environment using MS Visual Studio (the modified code and executables are available upon request).

3. Results and discussion

Based on the structural features of AAQs, we considered three models as their possible DNA binding mode: (i) minor/major groove binding, (ii) both groove binding and intercalation, (iii) bisintercalation; and carried out docking studies for each model. The purpose was to identify the most probable DNA binding mode by comparing predicted binding affinities of 49 AAQs with their corresponding experimental values for each model and see which model shows better correlation.

3.1. Model selection

It seems probable that the selectivity of the alkyl-linked diquinolines is a consequence of the non-intercalated chromophore interacting with the narrow minor groove [6]. In addition, AT base pair selectivity is a prominent feature of minor groove binding ligands [17]. Because of the above mentioned facts, we chose the crystal structure of the DNA dodecamer d(CGCAAATTTGCG)$_2$ complexed with propamidine [8] (PDB ID: 102D; resolution: 2.2 Å) which has a long AT tract of six base pairs in length with many potential binding sites in the DNA groove and a ligand with similar structural moieties to AAQs, as our groove binding model for the docking studies.

Since it was proposed by a previous study [6] that alkyl-linked diquinolines intercalate monofunctionally with quinoline ring posed on the edge between intercalative and non-intercalative binding and potency of some AAQs was comparable to adriamycin, we used the crystal structure of the DNA hexamer d(CGATCG)$_2$ complexed with adriamycin [9] (PDB ID: 1D12; resolution: 1.5 Å) as our groove binding plus intercalation model. In this complex the chromophore is intercalated at the CpG steps at either end of the DNA helix with the amino sugar extended into the minor groove. There is a sequence dependence of the binding of the amino sugar to the AT base pair outside the intercalation site.

Having two planar ring systems separated by a linker chain (Fig. 1), there is a possibility that AAQs show their effect by intercalating bifunctionally into DNA. We based our bisintercalation model on crystal structure of the DNA fragment d(CGCG)$_2$ complexed with ditercalinium [10] (PDB ID: 1D32; resolution: 1.7 Å). In this complex ditercalinium has a rigid

Table 2
Simulation results from the internal validation phase

DNA binding agent	FDE[a] (kcal/mol)	ΔG[b] (kcal/mol)	K_i[c] ($T = 298.15$ K)	Experimental K_i
Propamidine	−12.75	−9.55	9.98×10^{-8}	4.7×10^{-5}[d]
Adriamycin	−15.45	−13.99	5.55×10^{-11}	1.79×10^{-5}[e]
Ditercalinium	−23.14	−22.00	7.47×10^{-17}	5×10^{-8}[f]

[a] Final docked energy.
[b] Estimated free energy of binding.
[c] Estimated inhibition constant.
[d] Apparent binding constant determined using ethidium bromide displacement assay [26].
[e] Calculated from the results of voltammetry at pH 7.1 [27].
[f] Apparent binding constant at pH 5.0 which bisintercalation happens. At pH 7.4 monointercalation happens ($K_{ap} = 10^{-7}$)[28].

Table 3
Docking simulations results sorted by the pIC$_{50}$ values

Compound	102D[a]		1D12[b]		1D32[c]		pIC$_{50}$[d]	ΔG_{obs}[e]	Ref.[f]
	FDE[g]	ΔG[h]	FDE[g]	ΔG[h]	FDE[g]	ΔG[h]			
P24	−15.41	−11.85	−14.09	−10.08	−14.68	−11.27	7.84	−10.69	[4]
M19	−14.22	−10.21	−13.32	−8.95	−14.19	−10.10	7.78	−10.61	[4]
M10	−14.99	−10.96	−13.60	−9.17	−14.24	−9.87	7.45	−10.15	[1]
P3	−14.86	−11.30	−13.89	−10.37	−13.99	−10.85	7.44	−10.15	[4]
P19	−15.02	−10.56	−13.64	−8.92	−15.30	−10.32	7.44	−10.15	[1]
M16	−12.78	−9.93	−12.33	−9.24	−12.13	−9.10	7.23	−9.86	[4]
M18	−14.27	−11.09	−12.98	−9.73	−12.89	−9.67	7.08	−9.65	[4]
P18	−15.60	−12.04	−13.57	−9.61	−15.06	−11.55	7.02	−9.57	[3]
P22	−13.94	−11.29	−13.13	−10.54	−13.61	−10.99	6.90	−9.41	[1]
M13	−12.83	−10.35	−12.11	−9.50	−11.72	−9.12	6.86	−9.35	[4]
P17	−14.71	−10.72	−13.45	−9.19	−14.85	−11.78	6.83	−9.31	[3]
P16	−14.56	−9.60	−13.59	−8.64	−14.35	−9.05	6.80	−9.28	[3]
M7	−12.88	−10.86	−11.93	−9.96	−12.04	−10.53	6.80	−9.28	[3]
M6	−12.52	−9.68	−11.74	−8.91	−11.32	−8.68	6.77	−9.23	[3]
M8	−13.82	−10.11	−12.78	−8.72	−13.28	−9.54	6.74	−9.18	[3]
M1	−12.90	−10.10	−12.11	−8.71	−11.57	−8.66	6.69	−9.12	[3]
P21	−15.33	−11.69	−13.48	−8.83	−14.62	−10.32	6.58	−8.98	[3]
P23	−14.44	−11.70	−13.17	−10.09	−13.74	−10.78	6.56	−8.94	[4]
M14	−12.88	−10.35	−12.13	−9.52	−11.72	−9.12	6.50	−8.86	[4]
M9	−14.52	−10.41	−13.25	−9.09	−13.93	−9.81	6.47	−8.82	[3]
P2	−14.33	−11.60	−12.98	−10.21	−13.48	−10.48	6.39	−8.71	[4]
P4	−16.67	−12.21	−14.07	−9.30	−15.13	−10.63	6.24	−8.51	[4]
M5	−11.87	−9.35	−11.32	−8.45	−10.17	−7.74	6.19	−8.44	[3]
P15	−13.39	−10.91	−12.64	−9.55	−12.26	−9.92	6.16	−8.40	[3]
P5	−12.88	−10.72	−12.34	−9.82	−10.67	−8.79	6.08	−8.29	[3]
P1	−14.23	−11.57	−13.05	−10.22	−13.33	−10.75	6.04	−8.24	[4]
M3	−11.82	−9.39	−11.12	−8.49	−10.28	−7.89	5.93	−8.08	[3]
M4	−11.78	−9.28	−11.27	−8.71	−10.08	−7.80	5.93	−8.08	[3]
P12	−13.32	−11.23	−12.30	−9.90	−10.31	−7.79	5.92	−8.07	[3]
P13	−13.24	−10.65	−12.72	−10.14	−12.74	−10.17	5.89	−8.03	[3]
P20	−16.08	−10.51	−11.14	−9.59	−15.20	−10.62	5.84	−7.97	[3]
P26	−13.36	−12.12	−12.19	−7.72	−13.28	−11.07	5.84	−7.96	[1]
P8	−13.30	−11.12	−12.36	−10.01	−11.73	−9.40	5.82	−7.94	[3]
M17	−10.19	−7.29	−13.17	−10.28	−11.37	−8.51	5.75	−7.84	[4]
M21	−15.46	−11.20	−12.90	−9.13	−13.79	−10.42	5.74	−7.83	[1]
M23	−15.08	−12.61	−12.60	−10.26	−11.76	−9.28	5.63	−7.68	[1]
P25	−15.27	−12.24	−12.94	−8.90	−13.31	−9.49	5.32	−7.26	[1]
P14	−13.12	−9.63	−12.34	−8.59	−12.49	−9.99	5.29	−7.21	[3]
M22	−13.40	−10.23	−12.32	−9.86	−13.84	−9.83	5.29	−7.21	[1]
P6	−13.06	−10.95	−11.70	−9.72	−11.76	−9.49	5.15	−7.03	[3]
P7	−13.27	−10.91	−11.43	−9.34	−12.47	−9.24	4.99	−6.81	[3]
M20	−14.21	−10.87	−12.38	−9.74	−12.52	−9.92	4.99	−6.80	[1]
P9	−13.23	−10.89	−12.16	−9.62	−13.01	−10.68	4.92	−6.71	[3]
P10	−12.76	−10.02	−12.31	−9.98	−11.99	−10.65	4.91	−6.69	[3]
P11	−13.53	−11.20	−12.19	−9.73	−12.67	−10.38	4.89	−6.66	[3]
M2	−11.94	−9.44	−11.17	−8.68	−10.56	−7.88	4.87	−6.64	[3]
M11	−12.52	−10.31	−11.70	−9.43	−10.96	−8.76	4.87	−6.64	[4]
M12	−12.76	−10.35	−12.10	−9.51	−11.66	−9.10	4.83	−6.58	[4]
M15	−13.06	−10.60	−11.53	−8.98	−11.54	−8.87	4.79	−6.53	[4]

[a] Groove binding model based on the DNA dodecamer d(CGCAAATTTGCG)$_2$ complexed with propamidine (PDB ID: 102D).
[b] Groove binding plus intercalation model based on the DNA hexamer d(CGATCG)$_2$ complexed with adriamycin (PDB ID: 1D12).
[c] Bisintercalation model based on the DNA fragment d(CGCG)$_2$ complexed with ditercalinium (PDB ID: 1D32).
[d] Cologarithm of the molar concentration causing 50% growth inhibition of KB cells.
[e] Observed free energy change of binding calculated from pIC$_{50}$ using equation explained in the binding affinity prediction section.
[f] Reference to the article reporting pIC$_{50}$ value.
[g] Final docked energy (kcal/mol).
[h] Estimated free energy change of binding (kcal/mol).

linker to prevent self-stacking between chromophores and the DNA fragment is kinked (by 15°) and severely unwound (by 36°) with exceptionally wide major and minor grooves.

3.2. Binding affinity prediction

In the latest version of AutoDock, based on the traditional molecular force-field model of interaction energy, a new scoring function at the level of binding free energy was derived and adopted [13]. The total binding free energy was empirically calibrated based on the restriction of internal rotors, the global rotation, the translation and a set of coefficient factors. All empirical methods have to use a training set and therefore they suffer from it: the content of the training set will influence the final model. Unfortunately, there was no DNA–ligand complex among thirty protein-ligand complexes used as training set for the calibration of AutoDock empirical model [13]. As such, there is no provision made in AutoDock utilities like ADDSOL (and also AutoDockTools) to assign atomic desolvation terms to nucleic acid atoms acting as a target molecule. Consequently, free energy change of binding (ΔG) and the corresponding inhibition constant (K_i) predicted by AutoDock 3.0 for DNA–ligand complexes might be unreliable. As clearly stated in the AutoDock 3.0 original article [13], the energies used and reported by AutoDock should be distinguished: there are docked energies, which include the intermolecular and intramolecular interaction energies, and which are used during dockings; and predicted free energies, which include the intermolecular energy and the torsional free energy, and are only reported at the end of a docking. Because of the above mentioned restrictions, we decided to use both final docked energy (FDE: sum of the final intermolecular energy and final internal energy of ligand) and estimated free energy change of binding (ΔG: sum of the final intermolecular energy and torsional free energy) reported for each docking and see which one has a better correlation with experimental values. We converted between the inhibition constant, K_i, and the observed free energy change of binding, ΔG, using the equation:

$$\Delta G_{obs} = RT \ln K_i$$

where R is the gas constant, 1.987 cal K^{-1} mol^{-1}, and T the absolute temperature, assumed to be room temperature, 298.15 K.

3.3. Internal validation

In the internal validation phase, propamidine, adriamycin and ditercalinium (Fig. 2) were docked onto d(CGCAAATTT-GCG)$_2$, d(CGATCG)$_2$ and d(CGCG)$_2$ oligonucleotides, respectively, according to the above docking protocol. Three, thirteen and two of the first highest ranking poses (of 50 poses total) were clustered within 0.5 Å RMSD for propamidine, adriamycin and ditercalinium, respectively. The lowest energy poses for each case are shown in Fig. 3. After superimposing the experimental and predicted conformations, the RMSD were ∼1.4, ∼0.81 and ∼1.02 Å, respectively which is considered as successfully docked [18–20] and indicating that the parameters set for the AutoDock simulations are reasonable for reproducing the X-ray structures. Calculated FDEs, ΔGs and K_is and experimental K_is are summarized in Table 2. Using Spearman correlation coefficient, which calculates the correlation between two sets of rankings, it becomes evident that the correlation between experimentally measured K_is and calculated binding affinities is significant at 0.01 level. The results demonstrate that these in silico methods are quite robust and suitable for assessing the interaction of such ligands with DNA.

3.4. Binding model analysis

To select the most probable conformation of the complexes given by AutoDock we used quantitative and qualitative considerations. First, we choose the conformation with the lowest FDE as the starting point. Then the chosen conformation was analyzed qualitatively based on the location/orientation of the ligand in relation to the oligonucleotide. In the case that in the chosen conformation the ligand location/orientation was not in accordance with the corresponding DNA binding model (groove binding, groove binding and intercalation or bisintercalation), the docked complex was discarded and the conformation with the next FDE value was analyzed. This procedure was repeated until

Table 4
Correlation coefficients between calculated and experimental binding affinities for the three different DNA binding models

Pearson's r^2	102D[a]		1D12[b]		1D32[c]	
	FDE[d]	ΔG[e]	FDE[d]	ΔG[e]	FDE[d]	ΔG[e]
$r^2_{(ALL)}$[f]	0.125[*]	0.002	0.357[**]	0.006	0.199[**]	0.001
$r^2_{(PAAQ)}$[g]	0.254[**]	0.021	0.637[**]	0.002	0.342[**]	0.001
$r^2_{(MAAQ)}$[h]	0.055	0.006	0.219[*]	0.015	0.158	0.003

[a] Groove binding model (102D).
[b] Groove binding plus intercalation model (1D12).
[c] Bisintercalation model (1D32).
[d] Correlations between calculated final docked energy (kcal/mol) and experimental values.
[e] Correlations between estimated free energy change of binding (kcal/mol) and experimental values.
[f] The square of the correlation coefficients for all the 49 AAQs.
[g] The square of the correlation coefficients for the 26 phenyl-AAQs.
[h] The square of the correlation coefficients for the 23 methyl-AAQs
[*] Correlation is significant at 0.05 level.
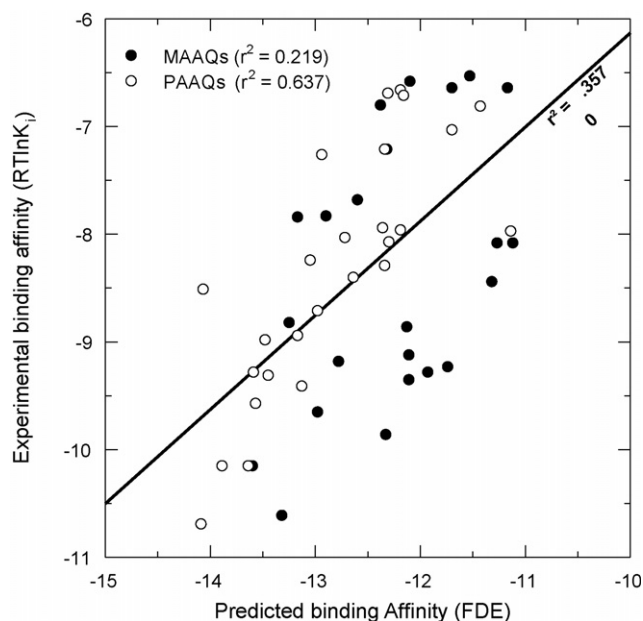[**] Correlation is significant at 0.01 level.

Fig. 4. The theoretically predicted binding affinity based on the final dock energy (FDE: kcal/mol) resulted from groove binding plus intercalation model (1D12) vs. experimentally measured ones for 49 AAQs used in this study. The solid line is from the regression fit. Methyl- and phenyl-AAQs are shown in solid and hollow dots, respectively.

we found a conformation in good harmony with the corresponding DNA binding model.

3.5. HIN2PDBQS utility

There is no support in AutoDockTools for assigning Kollman partial atomic charges to nucleic acids. Because of this inadequacy, we used HyperChem to assign partial atomic charges to DNA molecules. Kollman partial atomic charges assigned by HyperChem are based on the AMBER95 force field [21]; nevertheless, as stated in the AutoDock official web site (http://www.scripps.edu/mb/olson/doc/autodock/parameters.html), version 3 of the program is based on the AMBER86 [22]. In order to circumvent this problem, a dialog based utility named HIN2PDBQS for Win32 line of operating systems was developed in our group to convert AMBER95 partial atomic charges to either AMBER84 [23] or AMBER86. Ability to merge non-polar hydrogens and adding desolvation parameters are among other features of this utility. Source and binaries of HIN2PDBQS utility is available free of charge via Internet from: http://ams.iums.ac.ir/hin2pdbqs.

3.6. Docking simulations results

In docking simulations, 49 AAQs listed in Table 3 were docked onto d(CGCAAATTTGCG)$_2$, d(CGATCG)$_2$ and d(CGCG)$_2$ oligonucleotides according to the above docking protocol. Resulting FDE and predicted ΔG values for each model, along with experimental pIC$_{50}$ values (cologarithm of the molar concentration causing 50% growth inhibition of human-oral epithelial mouth carcinoma or KB cells) and corresponding ΔG_{obs} for each compound are presented in Table 3.
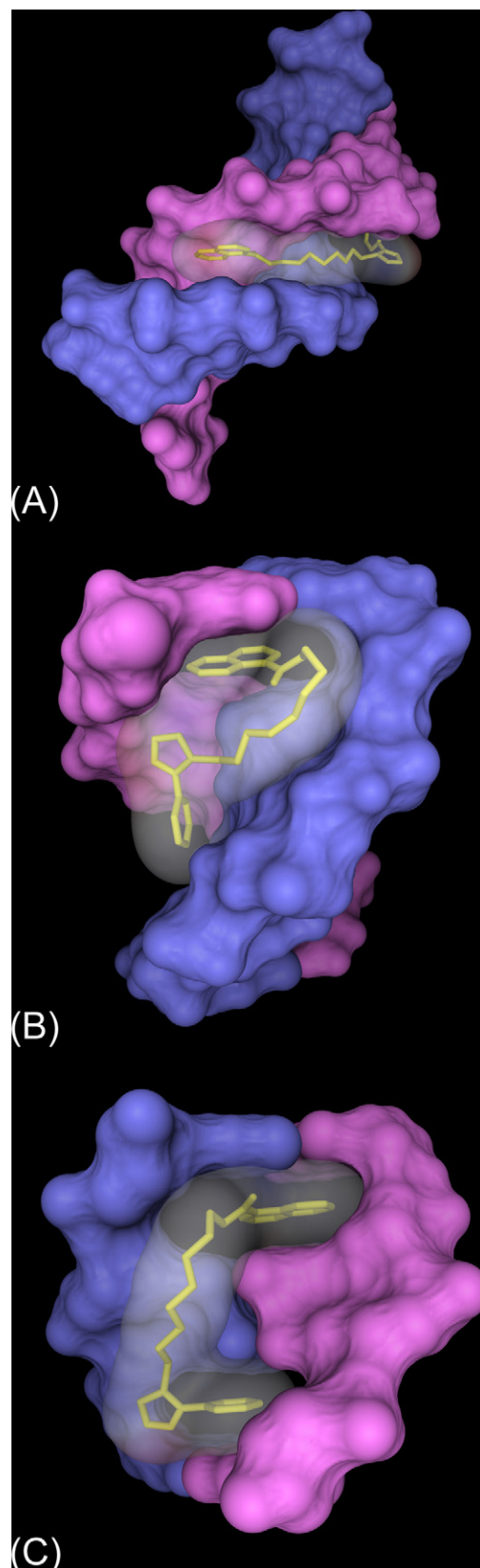
Fig. 5. Docking simulations results of the most potent compound in the series (P24). DNA structure rendered in blue and magenta as solvent-excluded surface (SES). Ligand structure rendered in yellow as stick model with transparent solvent-accessible surface (SAS). (A) Docking of P24 using groove binding model (102D). (B) Docking of P24 using groove binding plus intercalation model (1D12). (C) Docking of P24 using bisintercalation model (1D32).

The Pearson correlation coefficients between theoretically predicted and experimentally measured binding affinities for the three DNA binding models are summarized in Table 4. As the results in Table 4 indicate, there is a significant correlation between FDE values and experimental binding affinities for all the three DNA binding models, whereas no significant relationship between estimated free energy change of binding and experimental values is evident. This finding clearly demonstrates that FDE value reported by AutoDock is a better means for evaluating DNA–ligand interactions than estimated free energy change of binding.

By using FDE values for binding affinity prediction, it becomes evident that of the three DNA binding models selected in this study, groove binding plus intercalation model (1D12) shows a better correlation ($r^2 = 0.64$) than the other two models ($r^2 = 0.25$ for 102D and $r^2 = 0.34$ for 1D32) for PAAQ series (Fig. 4). These results make better sense when we consider results of a recent study [24] in evaluating performance of 12 different scoring functions in a benchmark of 100 protein–ligand complexes: the best performer was X-Score [25] ($r^2 = 0.41$) and the worst was AutoDock ($r^2 = 0.002$). It is also important to point out that only groove binding plus intercalation model (1D12) could rank P24 as the most potent compound among 48 other AAQs, which is quite remarkable. Fig. 5 displays the orientation of P24 compound produced by docking simulations for all three models.

Docking simulations using the three binding models show that despite differences in functional groups, the majority of ligands bind in a very similar fashion with minor variations in some intermolecular interactions within each model. Because of this fact, we used the compound (P15, located in the middle of Table 3; $n = 7$) with the closest pIC$_{50}$ value (6.16) to the average pIC$_{50}$ of the series (6.13) as a prototype for discussing important intermolecular interactions in each binding model.

In the groove binding model, P15 extends well in the AT-rich tract of the DNA minor groove, forming mostly simple hydrophobic interactions in quinolinic and linker chain regions with the two of the six AT base pairs (Fig. 6A). Two hydrogen bonds between two nitrogens of the azole ring and two adenine and thymine bases further stabilize the complex. There is no interaction between buried linker chain oxygen and AT base pairs. This is in contrast with P24 compound in which linker chain nitrogen forms two hydrogen bonds with two thymine residues.

In the groove binding plus intercalation model, quinolinic moiety of P15 intercalates between two consecutive CG base pairs, forming π-stacking interactions, while the linker chain and azole ring bind to the extended minor groove by forming simple hydrophobic interactions (Fig. 6B). Two hydrogen bonds between two nitrogens of the azole ring and the thymine base further stabilize the complex. Here again buried linker chain oxygen lacks any additional binding interactions with nearby guanine. This is again in contrast with P24 compound in which linker chain nitrogen forms a hydrogen bond with nearby guanine.

In the bisintercalation model, both the quinolinic moiety and the phenyl substituent connected to azole ring intercalate between two consecutive CG base pairs at the two ends of DNA
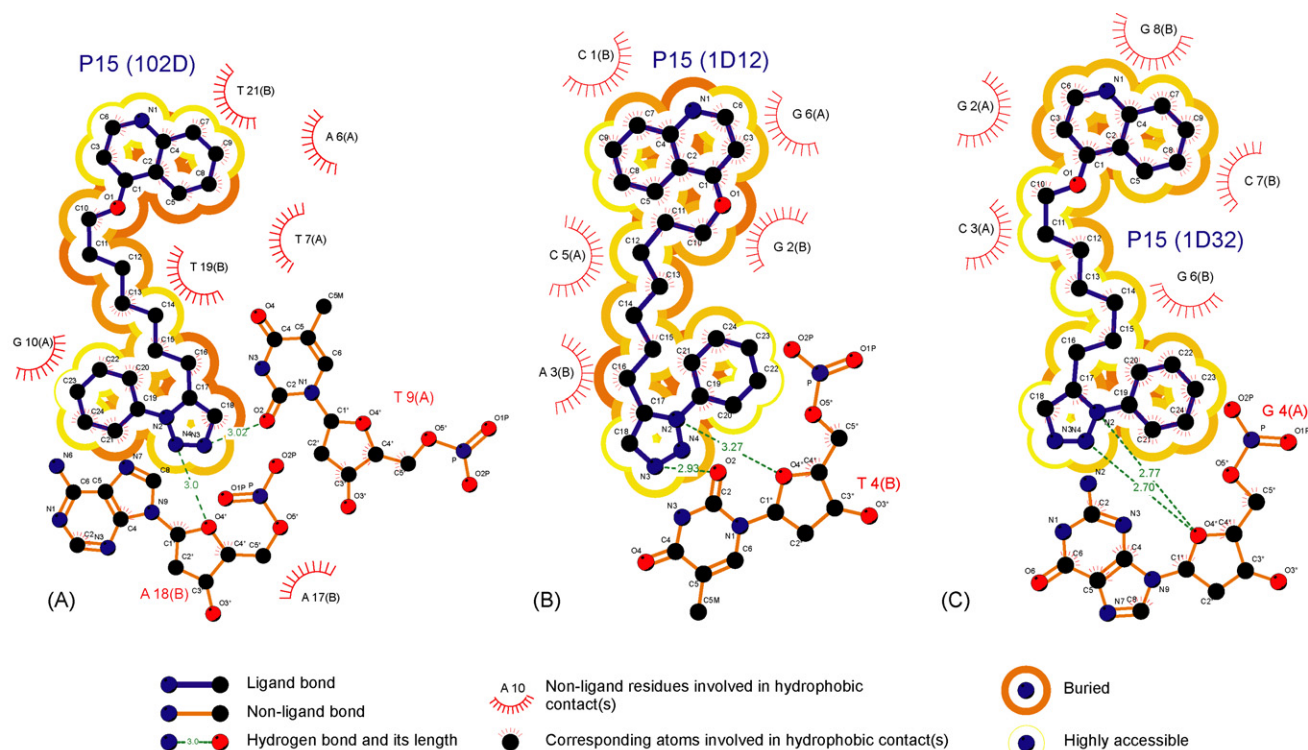
Fig. 6. Schematic two-dimensional representations of the binding interactions between the compound with closest pIC$_{50}$ value to the average pIC$_{50}$ value of the series (P15) and nucleotide residues of DNA molecules in each three binding models. (A) Groove binding model (102D). (B) Groove binding plus intercalation model (1D12). (C) Bisintercalation model (1D32). Binding interactions were calculated with the program LigPlot [29].

oligonucleotide, forming π-stacking interactions (Fig. 6C). There are two stabilizing hydrogen bonds formed between two nitrogens of azole ring and nearby guanine. Neither linker chain oxygen in P15 nor linker chain nitrogen in P24 form any additional interactions with nearby nucleotides.

4. Conclusions

The primary aim of the present study was to propose a model for the mode of action of AAQs as a DNA binding agents. Despite the existence of several deficiencies in AutoDock program in dealing with DNA as target macromolecules, in this study we presented a novel methodology for using the program in such studies. Our method can be applied to other research involving the use of AutoDock for DNA–ligand interactions. Our findings show that the most probable mode of action of PAAQs as DNA binding agents is via intercalation of quinolinic moiety between CG base pairs with the linker chain and azole moiety binding to the minor groove. In this regard, crystal structures of adriamycin and daunomycin in complex with DNA hexamer [9] (PDB IDs: 1D10 and 1D12) can act as good templates for further improvements of AAQ structures using structure-based drug design and *in silico* methods.

References

[1] M.D. Abel, H.T. Luu, R.G. Micetich, D.Q. Nguyen, A.B. Oreski, M.L. Tempest, M. Daneshtalab, Synthesis of azolylalkylquinolines with cytotoxic activity, J. Heterocycl. Chem. 33 (1996) 415–420.

[2] M.D. Abel, A.D. Cameron, C.M. Ha, C.A. Koski, H.T. Luu, R.G. Micetich, D.Q. Nguyen, M.L. Tempest, M. Daneshtalab, Novel azolylalkyloxy compounds with antipicornaviral activity, Antivir. Chem. Chemother. 6 (1995) 245–254.

[3] M.D. Abel, C.M. Ha, H.T. Luu, R.G. Micetich, D.Q. Nguyen, M. Nukatsuka, A.B. Oreski, M.L. Tempest, M. Daneshtalab, Cytotoxic quinolines (part 1). Azolylalkyloxy quinolines and 1-azolylalkyl-4(1H)-quinolones, Drug Des. Discov. 14 (1996) 15–30.

[4] M.D. Abel, C.M. Ha, H.T. Luu, R.G. Micetich, D.Q. Nguyen, M. Nukatsuka, A.B. Oreski, M.L. Tempest, M. Daneshtalab, Cytotoxic quinolines (part 2). Azolylalkylamino and-thio quinolines, Drug Des. Discov. 14 (1996) 31–42.

[5] M.D. Abel, R.G. Micetich, M. Nukatsuka, A.B. Oreski, M.L. Tempest, M. Daneshtalab, Cytotoxic quinolines (part 3). Synthesis of 1-azolylalkyl-4(1H)-quinolones as cytotoxic agents, Drug Des. Discov. 14 (1996) 115–127.

[6] W.D. McFadyen, W.A. Denny, L.P.G. Wakelin, Alkyl-linked diquinolines are monofunctional at-selective DNA-intercalating agents, FEBS Lett. 228 (1988) 235–240.

[7] X.-L. Yang, A.H.J. Wang, Structural studies of atom-specific anticancer drugs acting on DNA, Pharmacol. Therapeut. 83 (1999) 181.

[8] C.M. Nunn, S. Neidle, Sequence-dependent drug binding to the minor groove of DNA: crystal structure of the DNA dodecamer d(CGCAAATTTGCG)2 complexed with propamidine, J. Med. Chem. 38 (1995) 2317–2325.

[9] C.A. Frederick, L.D. Williams, G. Ughetto, G.A. van der Marel, J.H. van Boom, A. Rich, A.H. Wang, Structural comparison of anticancer drug-

[10] Q. Gao, L.D. Williams, M. Egli, D. Rabinovich, S.L. Chen, G.J. Quigley, A. Rich, Drug-induced DNA repair: X-ray structure of a DNA–dintercalinium complex, Proc. Natl. Acad. Sci. U.S.A. 88 (1991) 2422–2426.

[11] H.M. Berman, J. Westbrook, Z. Feng, G. Gilliland, T.N. Bhat, H. Weissig, I.N. Shindyalov, P.E. Bourne, The Protein Data Bank, Nucleic Acids Res. 28 (2000) 235–242.

[12] J. Gasteiger, M. Marsili, Iterative partial equalization of orbital electronegativity—a rapid access to atomic charges, Tetrahedron 36 (1980) 3219–3228.

[13] G.M. Morris, D.S. Goodsell, R.S. Halliday, R. Huey, W.E. Hart, R.K. Belew, A.J. Olson, Automated docking using a Lamarckian genetic algorithm and an empirical binding free energy function, J. Comput. Chem. 19 (1998) 1639–1662.

[14] F.J. Solis, R.J.B. Wets, Minimization by random search techniques, Math. Oper. Res. 6 (1981) 19–30.

[15] B.J. McConkey, V. Sobolev, M. Edelman, The performance of current methods in ligand-protein docking, Curr. Sci. 83 (2002) 845–856.

[16] R.X. Wang, Y.P. Lu, S.M. Wang, Comparative evaluation of 11 scoring functions for molecular docking, J. Med. Chem. 46 (2003) 2287–2303.

[17] W. Muller, F. Gautier, Interactions of heteroaromatic compounds with nucleic acids. A-T-specific non-intercalating DNA ligands, Eur. J. Biochem. 54 (1975) 385–394.

[18] H. Gohlke, M. Hendlich, G. Klebe, Knowledge-based scoring function to predict protein-ligand interactions, J. Mol. Biol. 295 (2000) 337.

[19] J.A. Erickson, M. Jalaie, D.H. Robertson, R.A. Lewis, M. Vieth, Lessons in molecular recognition: the effects of ligand and protein flexibility on molecular docking accuracy, J. Med. Chem. 47 (2004) 45–55.

[20] J.W.M. Nissink, C. Murray, M. Hartshorn, M.L. Verdonk, J.C. Cole, R. Taylor, A new test set for validating predictions of protein-ligand interaction, Proteins: Struct., Funct., Genet. 49 (2002) 457–471.

[21] W.D. Cornell, P. Cieplak, C.I. Bayly, I.R. Gould, K.M. Merz, D.M. Ferguson, D.C. Spellmeyer, T. Fox, J.W. Caldwell, P.A. Kollman, A 2nd generation force-field for the simulation of proteins, nucleic-acids, and organic-molecules, J. Am. Chem. Soc. 117 (1995) 5179–5197.

[22] S.J. Weiner, P.A. Kollman, D.T. Nguyen, D.A. Case, An all atom force-field for simulations of proteins and nucleic-acids, J. Comput. Chem. 7 (1986) 230–252.

[23] S.J. Weiner, P.A. Kollman, D.A. Case, U.C. Singh, C. Ghio, G. Alagona, S. Profeta, P. Weiner, A new force-field for molecular mechanical simulation of nucleic-acids and proteins, J. Am. Chem. Soc. 106 (1984) 765–784.

[24] C. Zhang, S. Liu, Q. Zhu, Y. Zhou, A knowledge-based energy function for protein–ligand, protein–protein, and protein–DNA complexes, J. Med. Chem. 48 (2005) 2325–2335.

[25] R. Wang, L. Lai, S. Wang, Further development and validation of empirical scoring functions for structure-based binding affinity prediction, J. Comput. -Aided Mol. Des. 16 (2002) 11.

[26] H.A. Johnson, N.R. Thomas, Polyhydroxylated azepanes as new motifs for DNA minor groove binding agents, Bioorg. Med. Chem. Lett. 12 (2002) 237.

[27] M.S. Ibrahim, Voltammetric studies of the interaction of nogalamycin antitumor drug with DNA, Anal. Chim. Acta 443 (2001) 63–72.

[28] D. Pelaprat, A. Delbarre, I. Le Guen, B.P. Roques, J.B. Le Pecq, DNA intercalating compounds as potential antitumor agents. 2. Preparation and properties of 7H-pyridocarbazole dimers, J. Med. Chem. 23 (1980) 1336–1343.

[29] A.C. Wallace, R.A. Laskowski, J.M. Thornton, Ligplot—a program to generate schematic diagrams of protein ligand interactions, Protein Eng. 8 (1995) 127–134.